Supporting Information

Printing Assembly and Structural Regulation of Graphene towards Three-dimensional Flexible Micro-Supercapacitors

Wenbo Li[a,b], Yonghe Li[c], Meng Su[a,b], Boxing An[d], Jing Liu[a], Dan Su[a], Lihong Li[a], Fengyu Li[a]*, Yanlin Song[a]*

[a] *Key Laboratory of Green Printing, Institute of Chemistry, Chinese Academy of Sciences (ICCAS), Beijing Engineering Research Center of Nanomaterials for Green Printing Technology, CAS Research/Education Center for Excellence in Molecular Sciences, Beijing 100190, P. R. China. *E-mail: ylsong@iccas.ac.cn, forrest@iccas.ac.cn*

[b] *University of Chinese Academy of Sciences, Beijing, 100049, P. R. China*

[c] *Institute of Microstructure and Property of Advanced Materials, Beijing University of Technology, Beijing 100124, P. R. China.*

[d] *School of Materials Science and Engineering, Shenyang Jianzhu University, Shenyang 110168, P. R. China*

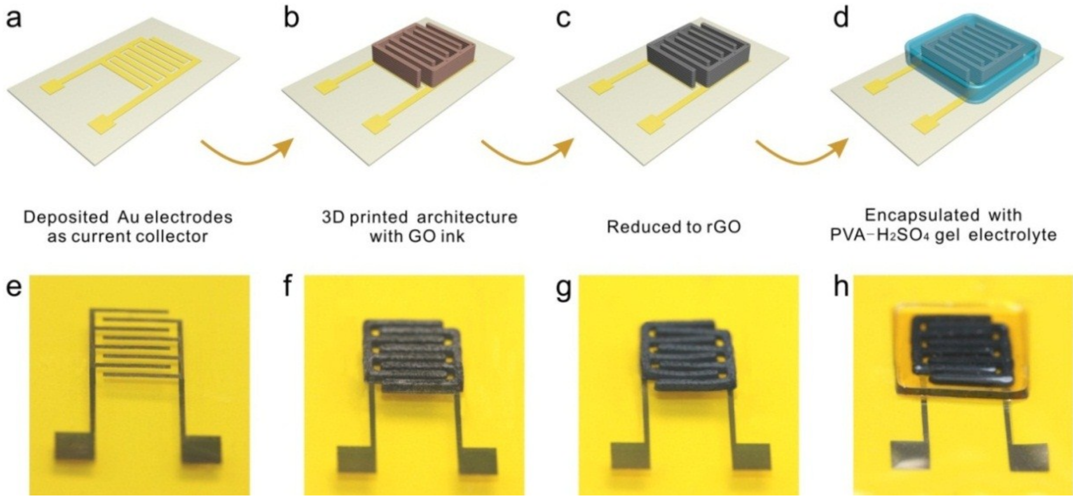

Fig. S1 Detailed fabrication process of the MSCs. Scheme (a−d) and photographs (e−h) illustrating the steps toward MSCs. Firstly, a gold layer is deposited on PI substrate as current collector (a, e). Then, interdigitated architecture is printed on top of Au layer with GO ink (b, f). The architecture is freeze dried and chemical reduced to rGO electrodes (c, g). Finally, the MSC is completed by packaging with gel electrolyte (d, h).

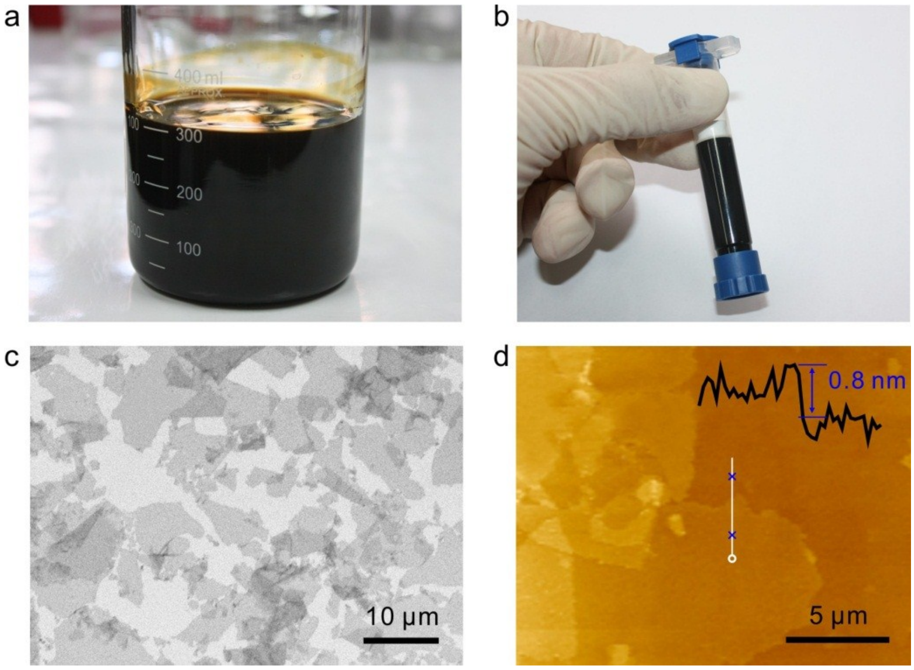

Fig. S2 Preparation of the GO based ink. (a) As-synthesized GO dispersion. (b) GO ink with concentration of 20 mg mL^{-1}. (c) SEM image of GO sheets, with average size of 15.6 μm. (d) AFM image of GO sheet, with thickness of ~ 0.8 nm, corresponding to the monolayer distribution.

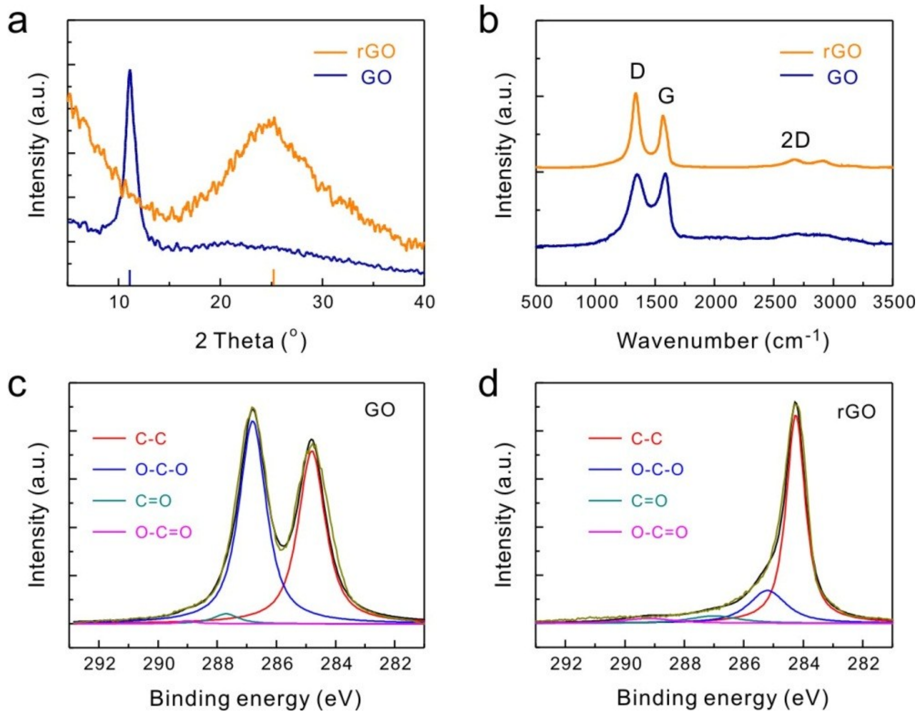

Fig. S3 Characterization of GO and rGO by XRD (a), Raman spectra (b), and XPS spectra (c, d). After reduction, the oxygen-containing groups significantly decreased, and the defects on the sheets are partially restored.

Table S1 BET surface area of the rGO electrode at varying T_f.

T_f (°C)	SA_{BET} ($m^2 \cdot g^{-1}$)
-50	243.22
-40	225.28
-30	198.13
-20	186.61
-10	163.75
0	261.12
10	141.57
20	129.28

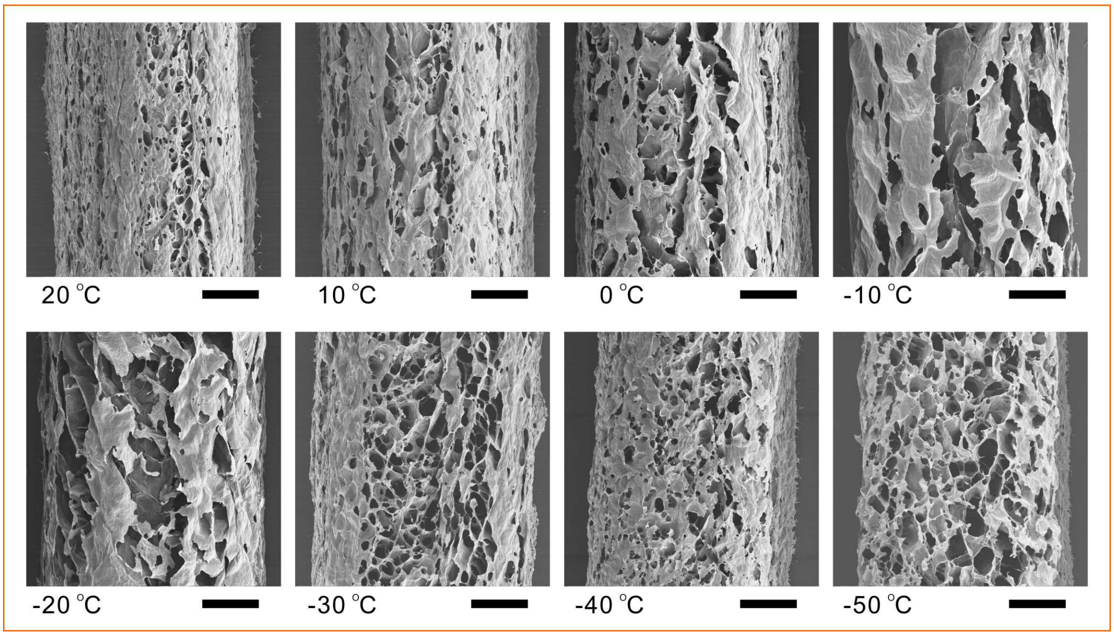

Fig. S4 Top view from SEM images of the MSCs, with T_f from 20 °C to -50 °C. Scale bars: 100 μm.

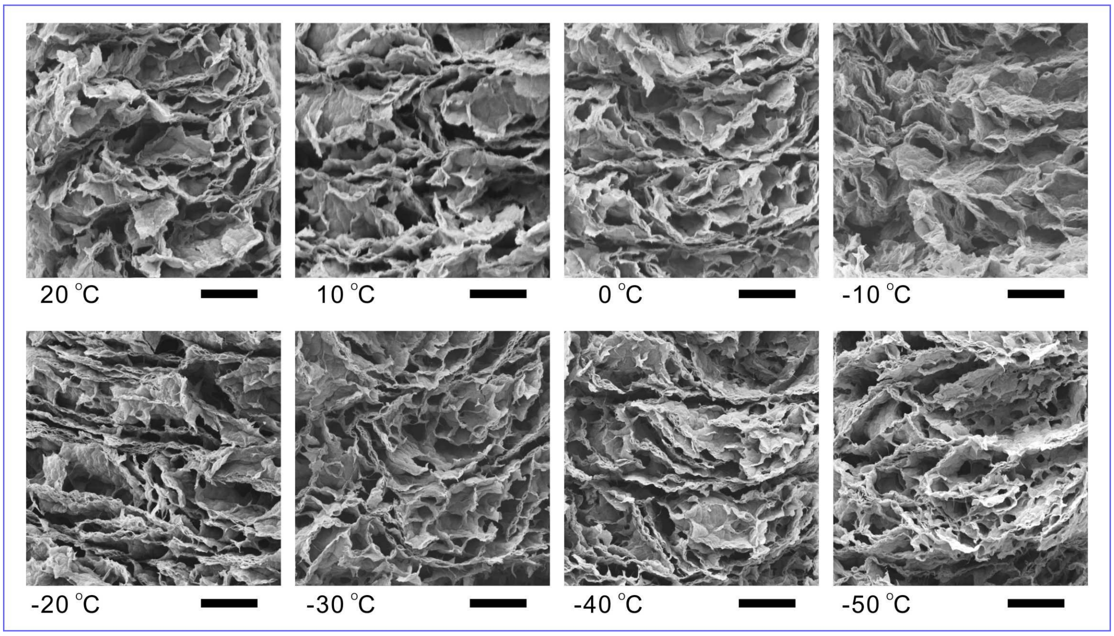

Fig. S5 Cross morphologies of the MSCs, with T_f from 20 ^{o}C to -50 ^{o}C. Scale bars: 100 μm.

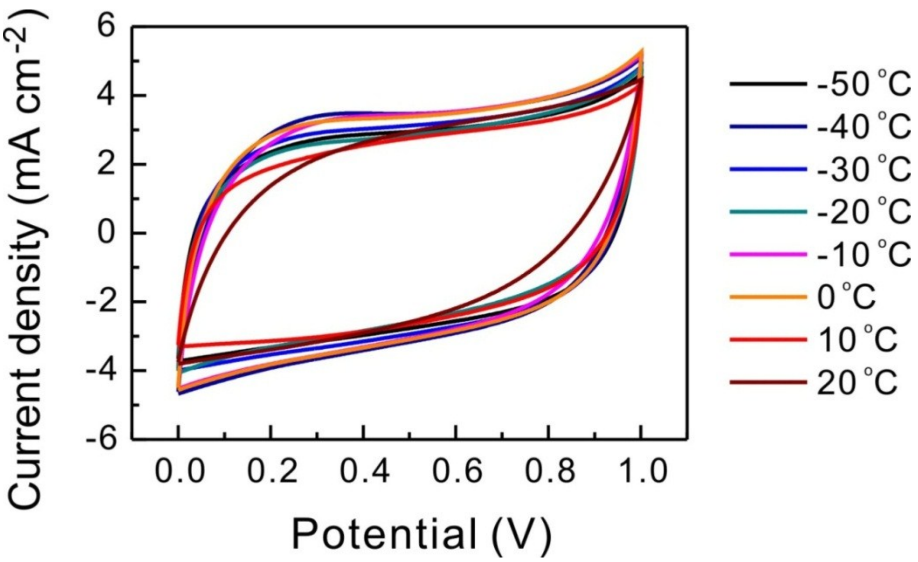

Fig. S6 CV curves of the MSCs with T_f from 20 °C to -50 °C, at a scan rate of 50 mV s^{-1}.

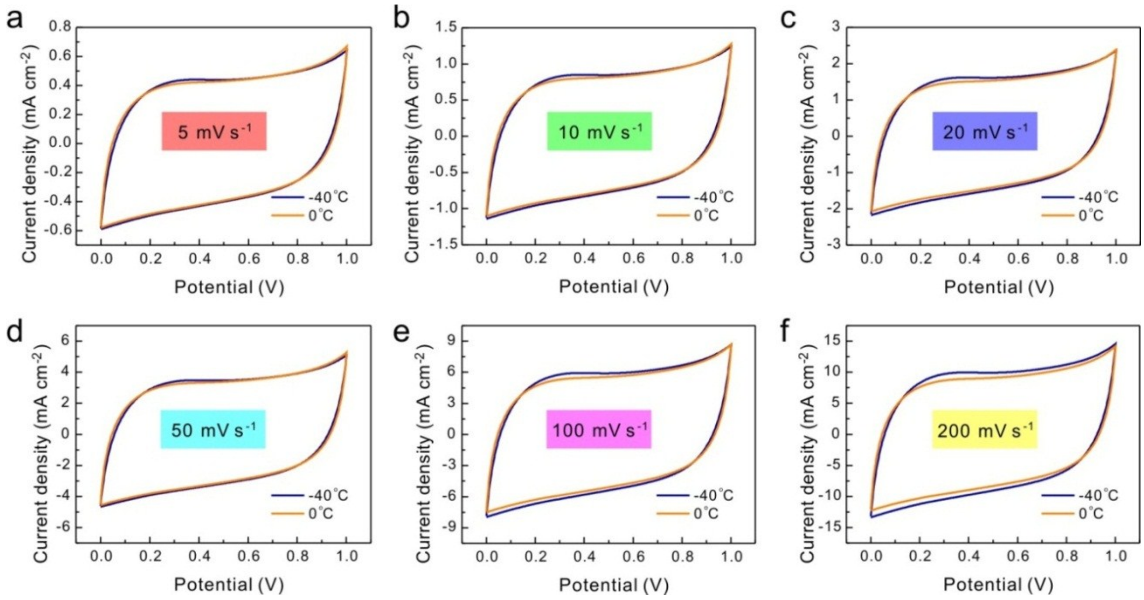

Fig. S7 (a−f) CV curves of the MSCs with T_f of -40 ^{o}C to 0 ^{o}C, at various scan rates from 5 to 200 mV s^{-1}.

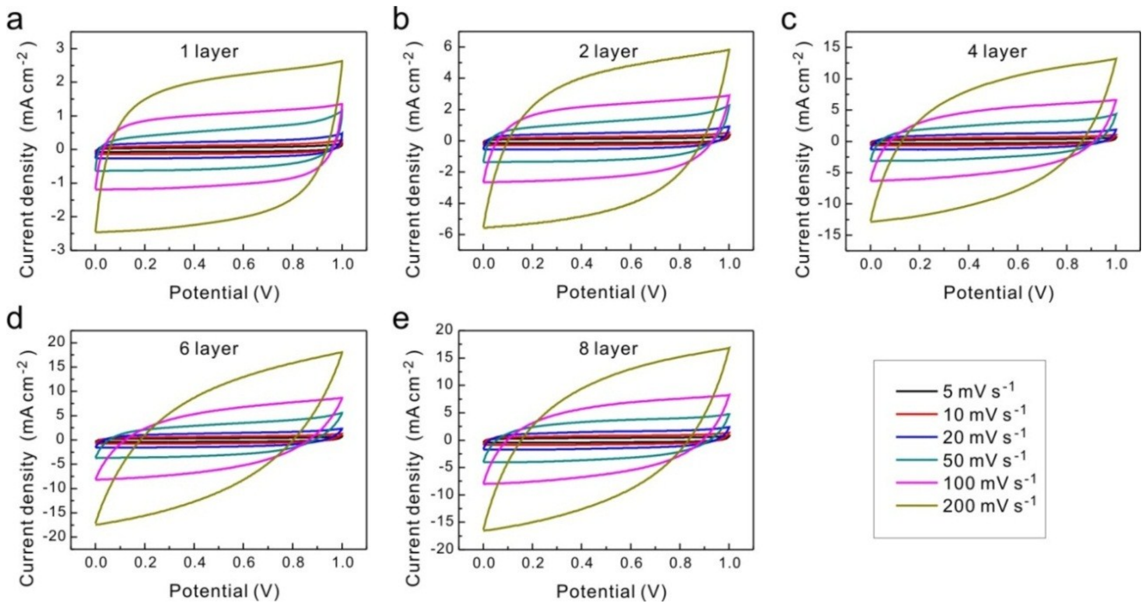

Fig. S8 (a−e) CV curves of the MSCs with 1−8 layers, at various scan rates from 5 to 200 mV s^{-1}.

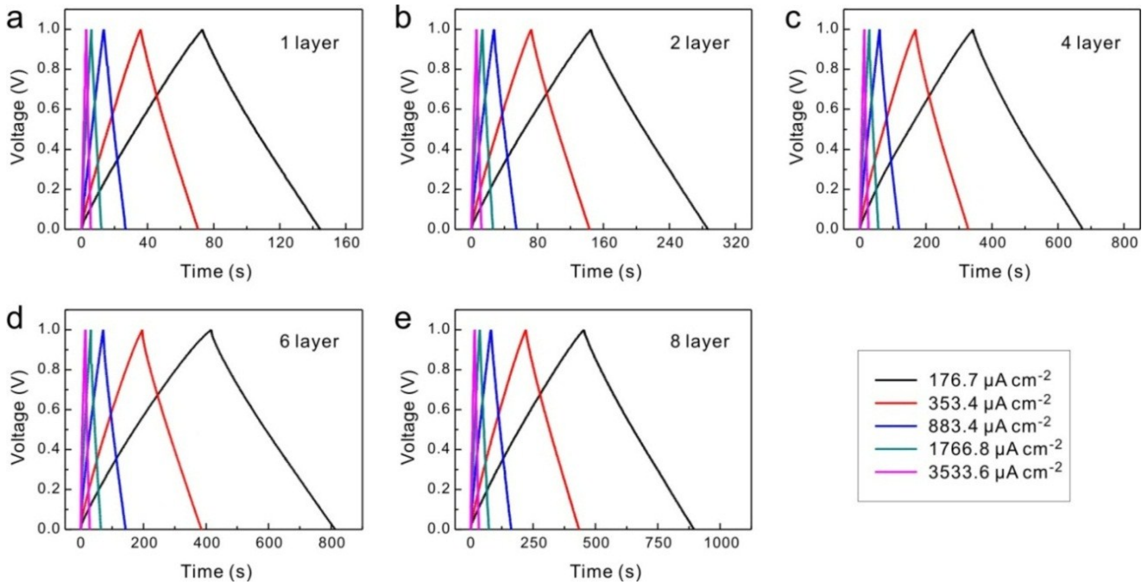

Fig. S9 (a−e) GCD profiles of the MSCs with 1−8 layers, at varying current densities from 176.7 to 3533.6 μA cm^{-2}.

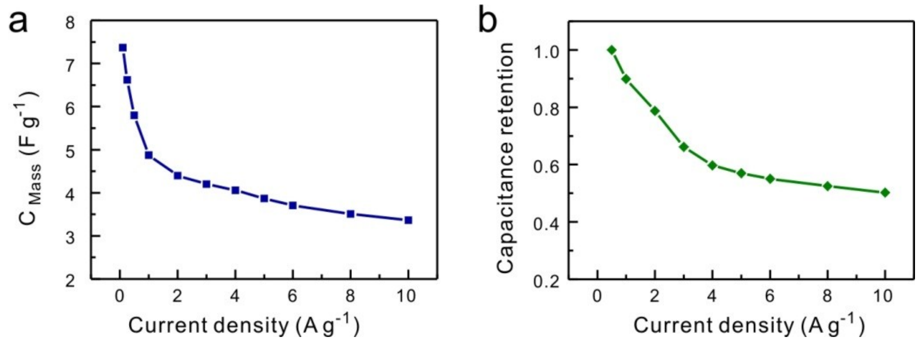

Fig. S10 (a, b) C_{Mass} and capacitance retention of MSCs calculated as a function of current density.

Table S2 Volumetric capacitive properties of various graphene supercapacitors

System	**Capacitance** (at highest current density)	**Rate capability**
Printed planar MSCs (ref. 10)	18.2 F cm^{-3} (3 A cm^{-3})	32% (0.06−3 A cm^{-3})
Inkjet-printed graphene MSCs (ref. 11)	5.0 F cm^{-3} (50 A cm^{-3})	54% (0.25−50 A cm^{-3})
Laser-scribed graphene MSCs (ref. 12)	1.83 F cm^{-3} (18.4 A cm^{-3})	60% (0.0168−18.4 A cm^{-3})
3D printed graphene supercapacitors with sandwich structure (ref. 48)	0.96 F cm^{-3} (2.6 A cm^{-3})	~ 62% (0.25−2.6 A cm^{-3})
3D printed graphene MSCs with interdigitated architecture (This work)	0.43 F cm^{-3} (1.14 A cm^{-3})	50% (0.06−1.14 A cm^{-3})

Note: All the data are calculated based on situation that the devices are operated with solid or quasi-solid state electrolyte.

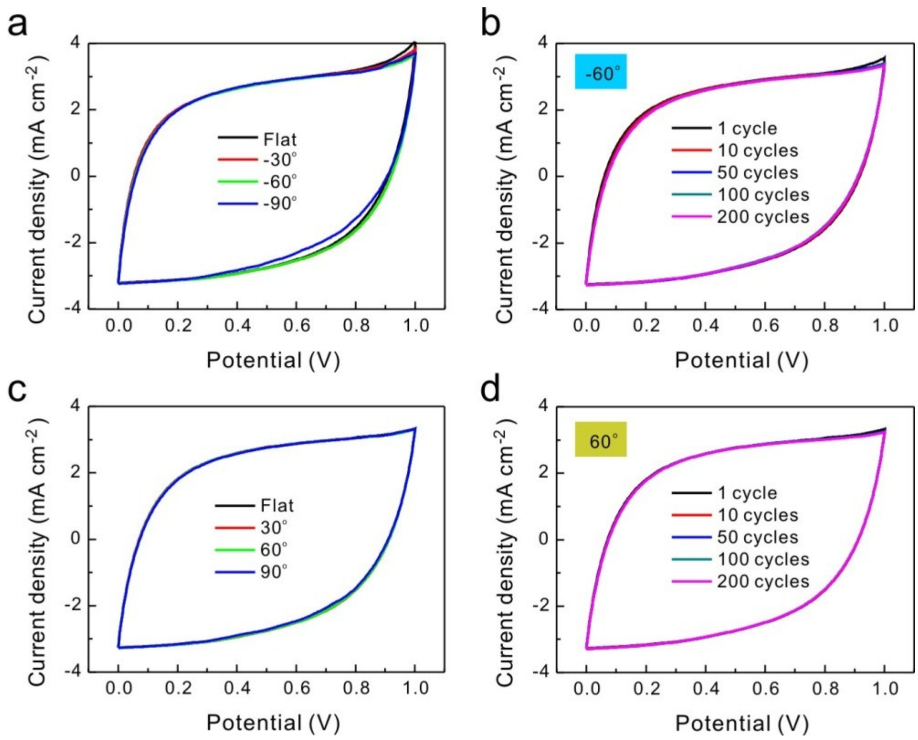

Fig. S11 Electrochemical performances of the MSCs by mechanical bending tests. (a) CV curves of the MSCs as a function of bending angle under compression from the flat state to -90°. (b) CV curves of the MSCs as a function of bending cycles under compression. (c) CV curves of the MSCs as a function of bending angle under tension from the flat state to 90°. (d) CV curves of the MSCs as a function of bending cycles under tension.

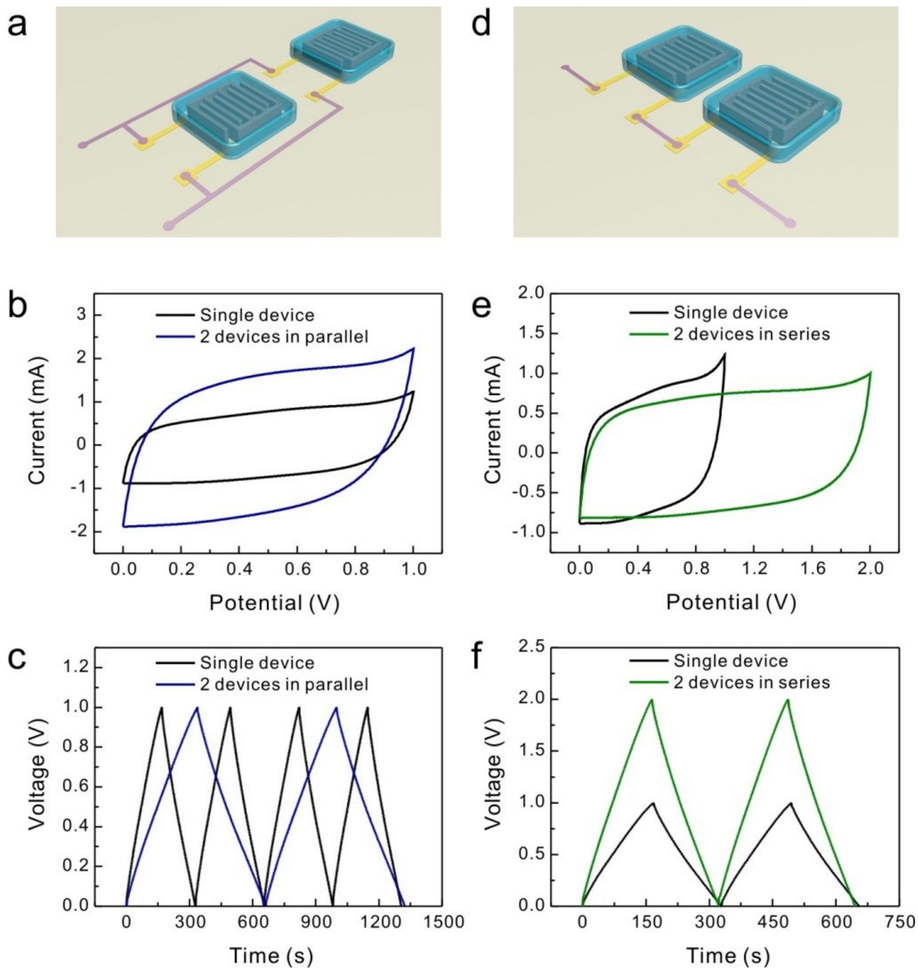

Fig. S12 Assembly of two MSCs connected in parallel and in series. (a) Schematic of two MSCs in parallel. (b, c) CV and GCD curves of the device shown in (a). (d) Schematic of two MSCs in series. (e, f) CV and GCD curves of the device shown in (d).

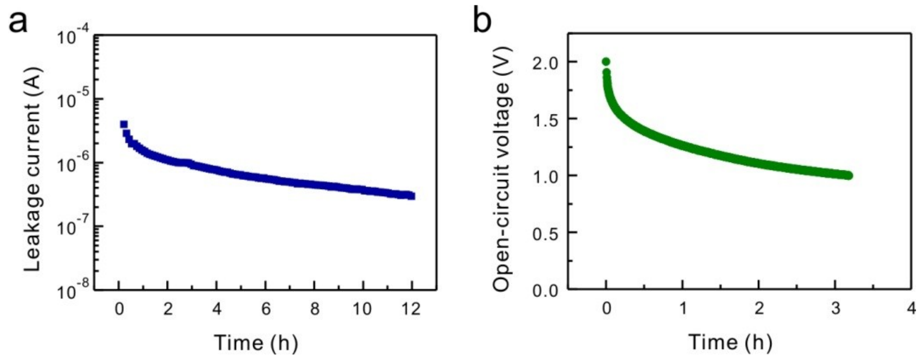

Fig. S13 (a) Leakage current of the MSCs with two devices connected in series. The measurement is operated at V_{max} for a period of 12 h. (b) Self-discharge plot of the series connected MSCs immediately after precharging to V_{max} till ½ V_{max}.

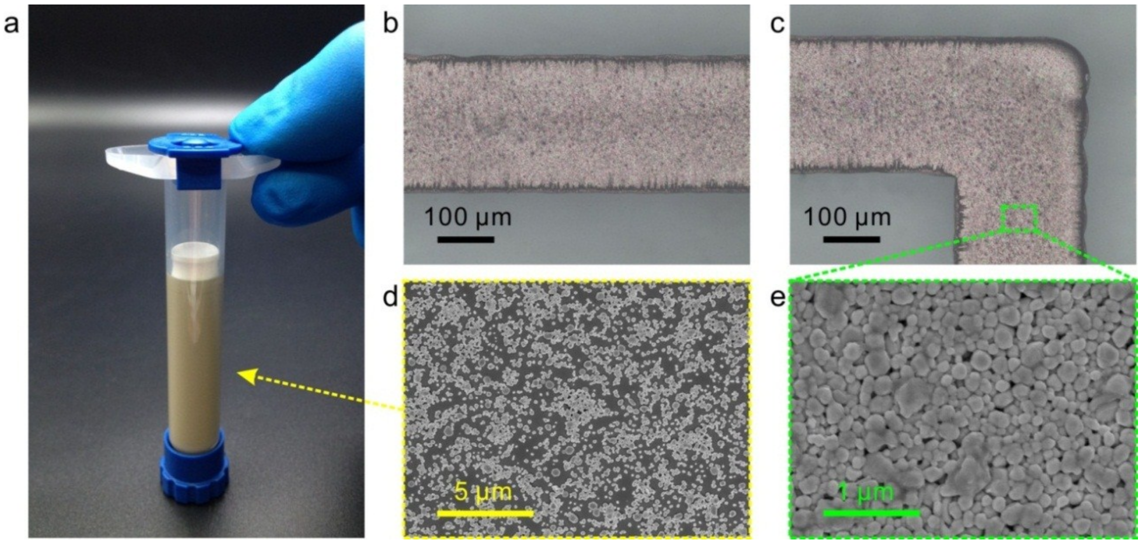

Fig. S14 The silver nanoparticles based ink for interconnection of the MSCs. (a) Photograph of the silver ink for direct writing. The ink has a silver concentration of 60 wt%. (b, c) Typical features printed by the ink. (d) SEM image showing the size distribution of the Ag nanoparticles, which have average diameter of ~ 100 nm. (e) SEM image showing the morphology from the printed lines. The Ag nanoparticles form efficient connection after sintering.